Direction of information flow in large-scale resting-state networks is frequency-dependent

Arjan Hillebrand[a,1], Prejaas Tewarie[a], Edwin van Dellen[a,b], Meichen Yu[a], Ellen W. S. Carbo[c], Linda Douw[c,d], Alida A. Gouw[a,e], Elisabeth C. W. van Straaten[a,f], and Cornelis J. Stam[a]

[a]Department of Clinical Neurophysiology and Magnetoencephalography Center, VU University Medical Center, 1081 HV Amsterdam, The Netherlands; [b]Department of Psychiatry, Brain Center Rudolf Magnus, University Medical Center Utrecht, 3508 GA Utrecht, The Netherlands; [c]Department of Anatomy and Neurosciences, VU University Medical Center, 1081 HV Amsterdam, The Netherlands; [d]Department of Radiology, Athinoula A. Martinos Center for Biomedical Imaging, Massachusetts General Hospital, Charlestown, MA 02129; [e]Alzheimer Center and Department of Neurology, VU University Medical Center, 1081 HV Amsterdam, The Netherlands; and [f]Nutricia Advanced Medical Nutrition, Nutricia Research, 3584 CT Utrecht, The Netherlands

Edited by Marcus E. Raichle, Washington University in St. Louis, St. Louis, MO, and approved February 24, 2016 (received for review August 8, 2015)

Normal brain function requires interactions between spatially separated, and functionally specialized, macroscopic regions, yet the directionality of these interactions in large-scale functional networks is unknown. Magnetoencephalography was used to determine the directionality of these interactions, where directionality was inferred from time series of beamformer-reconstructed estimates of neuronal activation, using a recently proposed measure of phase transfer entropy. We observed well-organized posterior-to-anterior patterns of information flow in the higher-frequency bands (alpha1, alpha2, and beta band), dominated by regions in the visual cortex and posterior default mode network. Opposite patterns of anterior-to-posterior flow were found in the theta band, involving mainly regions in the frontal lobe that were sending information to a more distributed network. Many strong information senders in the theta band were also frequent receivers in the alpha2 band, and vice versa. Our results provide evidence that large-scale resting-state patterns of information flow in the human brain form frequency-dependent reentry loops that are dominated by flow from parieto-occipital cortex to integrative frontal areas in the higher-frequency bands, which is mirrored by a theta band anterior-to-posterior flow.

information flow | phase transfer entropy | resting-state networks | magnetoencephalography | atlas-based beamforming

The brain is an extremely complex system (1–3) containing, at the macroscopic scale, interconnected functional units (4) with more-or-less specific information processing capabilities (5). However, cognitive functions require the coordinated activity of these spatially separated units, where the oscillatory nature of neuronal activity may provide a possible mechanism (6–9). A complete description of these interactions, in terms of both strength and directionality, is therefore necessary for the understanding of both normal and abnormal brain functioning.

Functional interactions may be inferred from statistical dependencies between the time series of neuronal activity at different sites, so-called functional connectivity (10). Indeed, interactions in large-scale functional networks have been observed using Electroencephalography, Magnetoencephalography (EEG/MEG) and functional Magnetic Resonance Imaging (fMRI) (e.g., refs. 11–14). However, as yet, little is known about the directionality of these interactions in large-scale functional networks during the resting state. Estimating directionality from fMRI is challenging due to its limited temporal resolution and indirect relation to neuronal activity (15, 16). In contrast, EEG studies in healthy controls have revealed a front-to-back pattern of directed connectivity, particularly in the alpha band (17–22), consistent with modeling studies that have shown that such patterns may arise due to differences in the number of anatomical connections (the degree) of anterior and posterior regions (22, 23). However, modeled patterns of information flow depend on the assumed strength of the underlying structural connections (22–24), and the observed EEG patterns strongly depend on the choice of reference (25), which may explain why, controversially, the reverse back-to-front pattern has also been observed in EEG (26–28). An important advantage of MEG over EEG in this context is that it is reference-free. Moreover, the large number of sensors (several hundreds) in modern whole-head MEG systems allow for sophisticated spatial filtering approaches to accurately reconstruct time series of neuronal activation across the cortex (29, 30). The directed functional connectome can subsequently be reconstructed by estimating information flow between these time series, using either model-based or data-driven approaches (31–34). Here, we used a recently introduced, sensitive, yet computationally efficient, data-driven measure of information flow, the phase transfer entropy (PTE) (35), to test the hypothesis that resting-state MEG data are characterized by a dominant front-to-back pattern in the alpha band. PTE was applied to MEG source-reconstructed eyes-closed resting-state data in a cohort of healthy subjects to characterize frequency-specific patterns of information flow in the human brain.

Results

Time series of neuronal activity were reconstructed by applying an atlas-based beamforming approach to eyes-closed resting-state MEG data from a cohort of 67 healthy subjects. The preferred direction of information flow between the 78 cortical regions in the automated anatomical labeling (AAL) atlas was estimated using the directed PTE (dPTE). The average information flow between a region and all other regions was first computed, resulting in a single estimate of preferred direction of information flow (outgoing or incoming) for each region (Fig. 1). Based on this pattern, the

Significance

A description of the structural and functional connections in the human brain is necessary for the understanding of both normal and abnormal brain functioning. Although it has become clear in recent years that stable patterns of functional connectivity can be observed during the resting state, to date, it remains unclear what the dominant patterns of information flow are in this functional connectome and how these relate to the integration of brain function. Our results are the first to describe the large-scale frequency-specific patterns of information flow in the human brain, showing that different subsystems form a loop through which information "reverberates" or "circulates." These results could be extended to give insights into how such flow optimizes integrative cognitive processing.

Author contributions: A.H., E.v.D., L.D., A.A.G., E.C.W.v.S., and C.J.S. designed research; A.H., P.T., M.Y., E.W.S.C., L.D., and C.J.S. performed research; A.H., P.T., M.Y., and C.J.S. contributed new reagents/analytic tools; A.H., P.T., M.Y., E.W.S.C., and L.D. analyzed data; and A.H., P.T., E.v.D., M.Y., E.W.S.C., L.D., A.A.G., E.C.W.v.S., and C.J.S. wrote the paper.

The authors declare no conflict of interest.

This article is a PNAS Direct Submission.

[1]To whom correspondence should be addressed. Email: a.hillebrand@vumc.nl.

This article contains supporting information online at www.pnas.org/lookup/suppl/doi:10.1073/pnas.1515657113/-/DCSupplemental.

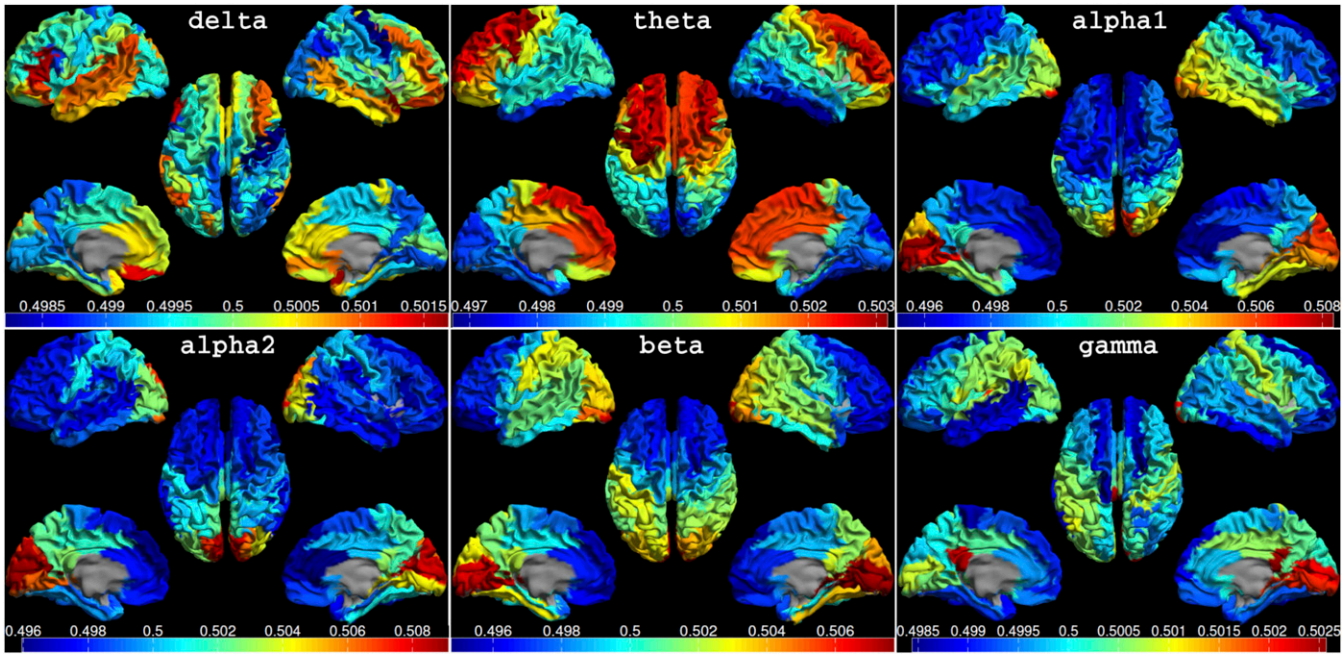

Fig. 1. Mean dPTE for each ROI displayed as a color-coded map on the parcellated template brain, viewed from, in clockwise order, the left, top, right, right midline, and left midline. Note the smooth global patterns of preferential information flow in the higher-frequency bands (alpha1 to beta), consisting of posterior regions that are leading anterior regions. The opposite pattern was observed in the theta band. Hot and cold colors indicate information outflow and inflow, respectively. See Fig. S1*A* for the connectivity matrices.

posterior–anterior index (PAx) was computed to establish if there was consistent information flow in the posterior–anterior direction. The flow between pairs of regions was subsequently examined in more detail (Fig. 2).

Fig. 1 reveals smooth global patterns of preferential information flow in the alpha1 (8–10 Hz), alpha2 (10–13 Hz), and beta (13–30 Hz) bands, consisting of posterior regions that are leading anterior regions [PAx = 0.39, 0.42, and 0.55 ($P < 0.001$), respectively]. The opposite pattern was observed in the theta (4–8 Hz) band (PAx = −0.50, $P < 0.001$). The patterns in the gamma (30–48 Hz) and delta (0.5–4 Hz) bands were more dispersed [although still significant ($P < 0.001$); PAx = 0.26 and −0.29, respectively]. We describe the results for the alpha2 and theta band in more detail below, as the patterns for these bands (*i*) were most pronounced and (*ii*) resulted in high PAx values.

It can be seen in Fig. 2 and Tables S2 and S4 that, in the alpha2 band, the strongest information flow was from posterior regions, including the (primary) visual areas and posterior parts of the default mode network (DMN), to anterior cingulate, frontal, and temporal regions. The 500 strongest outgoing connections all started in precuneus, superior, middle, and inferior occipital gyrus, calcarine fissure, cuneus, lingual gyrus, and posterior cingulate; the areas that received most of these connections were, in rank order, left medial superior frontal gyrus; right inferior frontal gyrus and right anterior cingulate; right superior frontal gyrus (dorsal and medial); left superior frontal gyrus (dorsal); and left superior frontal gyrus (medial orbital), left anterior cingulate, right

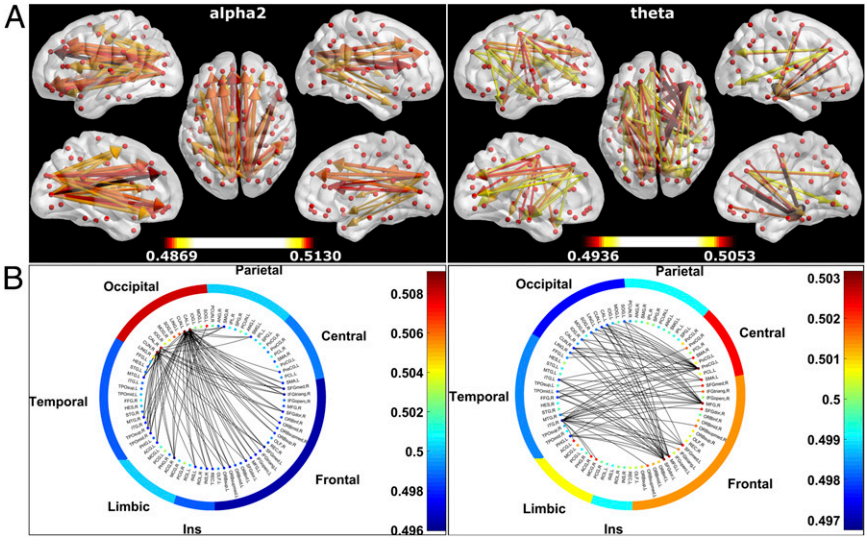

Fig. 2. Preferred direction of information flow between regions. (*A*) Preferential information flow for the alpha2 and theta band displayed on the template brain using BrainNet Viewer (version 1.5), viewed from, in clockwise order, the left, top, right, right midline, and left midline. Colors and line thickness indicate the dPTE values (lower and upper thresholds: [0.4892, 0.5108] and [0.4955, 0.5045] for the alpha2 and theta bands, respectively), and arrows indicate the preferred direction of information flow. Thresholds were chosen to highlight the dominant patterns formed by the information streams between regions; for statistically thresholded images, we refer to Fig. S1*B*. (*B*) Preferential information flow for the alpha2 and theta bands displayed as circular plots (after ref. 22). The color of each node indicates the mean dPTE value for that ROI. The full names of the ROIs are given in Table S1. The nodes were grouped as frontal lobe, central regions, parietal lobe, occipital lobe, temporal lobe, limbic region, and Insula (Ins), with the color of each group indicating the mean dPTE value for the group. The interior shows the connections between nodes (threshold as in *A*). See also Tables S2–S5.

supramarginal gyrus, right temporal pole (superior temporal gyrus), and the right insula. For the theta band (Fig. 2 and Tables S3 and S4), the pattern was more dispersed, with the strongest and most frequent connections between frontal and temporal regions, but also with many other regions showing (only) a few strong connections. Out of the 500 strongest outgoing connections, the outgoing connections started most frequently in (rank-ordered) left precentral gyrus; left superior frontal gyrus (dorsolateral); right middle frontal gyrus; left middle frontal gyrus; left superior frontal gyrus (medial) and left supplementary motor area; right supplementary motor area; left anterior cingulate and right superior frontal gyrus (dorsolateral); and right anterior cingulate and the right median cingulate. The most frequent receiving areas were right inferior temporal gyrus; right cuneus; left cuneus, left parahippocampal gyrus, and right fusiform gyrus; left calcarine fissure; left inferior temporal gyrus; left temporal pole (middle temporal gyrus); and left superior occipital gyrus and the right inferior occipital gyrus. Note that some of the most frequent sending regions in the alpha2 band tended to be frequent receivers in the theta band (Table S5). A similar effect, although less pronounced, was seen for the most frequent sending regions in the theta band: These were also often frequent receivers in the alpha2 band. Indeed, there was a significant negative correlation between the upper triangles of the dPTE matrices (Fig. S1*A*) in the alpha2 and theta band [$r(3,001) = -0.57$, $P < 0.001$].

To aid the interpretation of our results, we performed several extra analyses, which are described in *Supporting Information*: We compared results obtained for the eyes-closed condition to those obtained for the eyes-open condition, revealing similar patterns of information flow (Fig. S2). Similarly, these patterns, albeit with lower spatial resolution, were also found at the sensor level (Fig. S3), confirming that the observed patterns were not an artifact of the source reconstruction approach. In addition, we compared dPTE to another directional measure, the directed Phase Lag Index (dPLI) (23), which is based on phase differences rather than information flow (Fig. S4). Importantly, we also showed that these patterns of phase differences in a toy system of coupled Rössler oscillators depend on the global strength of the underlying structural connections, whereas dPTE revealed the correct patterns of information flow, independent of the coupling strength (Fig. S5). Finally, we estimated the relation between relative power and dPTE, as well as the effect of the choice of beamformer approach (Fig. S6).

Discussion

We have demonstrated, for the higher-frequency bands (8–30 Hz), dominant posterior-to-anterior patterns of information flow in an eyes-closed resting state from regions in the parieto-occipital lobe toward frontal areas. In contrast, a pattern of anterior-to-posterior flow was found in the theta band, involving mainly regions in the frontal lobe that were sending information to a more distributed network. Interestingly, strong senders of information in the alpha2 band were also often receivers of information in the theta band, and vice versa, suggesting a frequency-specific loop of information flow in the human brain.

Posterior regions of the DMN were found to be strong senders of information in the higher-frequency bands (8–30 Hz), and frequent receivers in the theta band. The DMN is strongly activated during the resting state (see also Fig. S6*B*), and has putatively been linked to spontaneous cognition (internal mentation) and/or general unconscious low-level attention to the external world (36, 37). At least two distinct interacting subsystems play a role in the DMN: one temporal system involved in memory processes, and a fronto-parietal system involved in self-relevant mental simulations (36). Our observation of a dominant posterior-to-anterior pattern of information flow in the higher-frequency bands between parieto-occipital regions and frontal regions, as well as an anterior-to-posterior pattern from frontal regions to temporal and posterior regions in the theta band, suggests that these subsystems form a loop (Table S5), or cell assembly (38, 39), through which information "reverberates" or "circulates." The observation that the theta band is important for memory processes in frontal and hippocampal areas further supports this idea (40, 41). A counterargument against such interpretations of our results is our observation that not only the posterior part of the DMN is involved in the posterior-to-anterior flow, but also, and most strongly, regions in the visual cortex. Therefore, the interpretation of the current findings can also be placed in a broader context, superseding the sole role of the DMN with respect to the observed patterns. The observation of a mirrored flow of information is reminiscent of reentry in neural systems as a mechanism for integration of brain function (42).

Recent hypotheses have stressed the importance of both alpha and theta connectivity in attention, where theta band connectivity from the medial frontal cortex to various regions plays a key role in inducing control from higher association areas over lower-level, perceptual processes, but also over the DMN (43). Our theta band findings seem to be in line with this theory, as it may explain why we found distributed theta band information flow from frontal areas to various regions, including the DMN. At the same time, this model predicts that anterior-to-posterior alpha connectivity provides a gating mechanism for attention, because top-down modulation by alpha could inhibit irrelevant activity (43, 44). This may seem to be in disagreement with our findings of a posterior-to-anterior dominant pattern of information flow in the alpha band, although it is possible that the enhanced bottom-up signaling in the alpha band is in itself a consequence of enhanced top-down signaling in the theta band (45). Moreover, one should take into consideration that our recordings were resting state and not task-based, and that neuronal signatures of different forms of attention (46) are assumed to be related but can have different spatiotemporal and frequency contents. The observed posterior-to-anterior information flow during the resting state is likely to be a signature for internal attention rather than for attention to external stimuli [also supported by our finding that opening the eyes during the resting state did not alter the dominant patterns of information flow (Fig. S2)]. These ideas could be tested in future task-based studies, where the exact role and direction of fronto-posterior connections could be analyzed for different forms of attention.

Alternatively, the oppositely directed propagated electrophysiological activity in different frequency bands could play a role in contexts other than attention (47), such as memory consolidation (48). Our results (Fig. 2) are, for example, consistent with animal recordings that have shown cortico-hippocampal propagation at low frequencies and cortico-cortical propagation at higher frequencies (49). Similarly, bottom-up and top-down influences through distinct fast- and slow-frequency channels have also been reported for the visual system (45, 50). Although these observations from task-based invasive animal recordings suggest that similar mechanisms may play a role during noninvasive resting-state recordings in humans, more work is needed to further elucidate the functional role of resting-state information flow through distinct frequency channels.

An alternative explanation for the observed stable patterns of information flow may come from the topological properties of the underlying structural network, as recent modeling work has suggested. In particular, highly connected regions in the network, so-called hubs, become phase-lagging with respect to nonhub regions (22, 23). Brain networks have their strongest hubs in posterior regions (36, 51), which would hence lead to a front-to-back pattern of phase differences. However, simply changing the global strength of the underlying structural connections may reverse this pattern (Fig. S5), indicating that patterns of phase differences should not be confused with patterns of directed connectivity or, indeed, information flow. Instead, one could hypothesize that the net outflow of information

from posterior regions is due to an increase in encoded information at higher firing rates (52), as simulations have shown that hubs also possess the highest levels of neuronal activity in the network, that is, the highest firing rates (53) and the highest power (22, 53).

Another factor that may have contributed to the discrepancy between our observed posterior-to-anterior pattern in the alpha band and the reverse pattern that was hypothesized on the basis of previous EEG studies in healthy subjects (refs. 17–22, but see refs. 26–28) is that the patterns of directionality in EEG strongly depend on the choice of reference (25). MEG, in contrast, is reference-free. Interestingly, we did not observe any consistent patterns of phase differences between anterior and posterior regions in any of the frequency bands in our source-reconstructed MEG data (Fig. S4). Finally, the artifact caused by the electrocardiogram (ECG) can cause consistent patterns of phase differences at the sensor level (54), because the artifact can be modeled as a rotating source (55). Application of beamforming not only allows for the reconstruction of information flow at the cortical level but also removes the ECG artifact (55), especially in combination with temporal extension of Signal Space Separation (tSSS) (56).

We observed a strong positive correlation between the patterns of dPTE and those of relative power [*dPTE Versus Relative Power (Centroid Beamformer)*], particularly for the alpha bands. It is therefore possible that the observed patterns of information flow are a direct consequence of differences in signal-to-noise ratio (SNR) between anterior and posterior regions, although the strong negative correlation between dPTE and relative power in the gamma band shows, at least, that this would not always be the case. Moreover, PTE is based on phase information and should therefore be relatively insensitive to differences in power or SNR (ref. 35, but see ref. 57). In addition, in our Rössler simulations (Fig. S5), there was a consistent pattern of information flow that did not depend on power differences. Furthermore, patterns of information flow observed in the experimental data for the eyes-open condition, i.e., when occipital alpha has low power, were similar to those obtained for the eyes-closed condition. Finally, modeling work suggests that the relationship between power and directionality may not simply be caused by differences in SNR but may be due to a neuronal mechanism that drives this correlation (52). Akam and Kullmann (52) showed that the amount of synchronous activity in a sending neuronal population, reflected in the amplitude of oscillations, is strongly related to the amount of information available to the receiving neuronal population. At the same time, interneuron motifs within the receiving neuronal population can act as bandpass filters to selectively gate incoming signals. This selective signal-gating mechanism could explain the strong positive correlation between amplitude and dPTE in our study, but it also explains why this correlation is not perfect, as the amplitude of the sending population itself is not the only prerequisite for routing information: There is also the sensitivity of receiving populations. However, given the mesoscopic level at which the analysis was performed and the infancy of this field, future modeling approaches need to include the influence of global structural topology (22–24) and inhomogeneity of neuronal populations to systematically study how patterns of information flow depend on frequency, power, SNR, and the role of regions within the network. Moreover, experimental studies should investigate if, and how, these patterns of information flow optimize integrative cognitive processing. An interesting hypothesis is, for example, that interruptions in the alpha–theta circular flow of information lead to poorer cognition.

Our results give direction to future studies on information flow in the human brain. Here, we analyzed the different frequency bands separately, and found posterior-to-anterior flow of information in the higher-frequency bands (alpha1, alpha2, and beta band), and anterior-to-posterior flow in the theta band, where some regions were frequent senders in one frequency band and frequent receivers in other frequency bands. Cross-frequency interactions, i.e., information flow across different frequency bands, were not studied directly, and our interpretation of the results in terms of a reentry loop of information flow should be accepted provisionally. Such cross-frequency interactions could be studied by applying the PTE to data filtered in different frequency bands for the senders and receivers (35). In addition, we only estimated information flow for relatively long time windows, such that we could not establish whether a single region switched from a sending to receiving state on short time scales or whether a region was simultaneously a sender in one frequency band and a receiver in another, consistent with the idea of oscillatory multiplexing for selective communication (58). This could be addressed by developing a dynamic dPTE approach.

Our approach, a combination of an atlas-based beamformer and PTE, revealed stable frequency-specific patterns of information flow in the healthy human brain. Future work should investigate how these patterns are disrupted in neurological disease, and how these disruptions relate to disease severity and cognitive performance.

Methods

Participants and Recording Protocol. Data from 67 healthy controls were analyzed. These data formed part of two cohorts in studies on Multiple Sclerosis (MS) at the VU University Medical Center (VUmc) MS Center (59–61), for which approval was obtained from the Medical Ethical Review Committee of VUmc, whose ethics review criteria conformed to the Helsinki declaration. All subjects gave written informed consent before participation.

Anatomical images of the head were obtained on a 3.0T whole-body MRI scanner (GE Signa HDxt), using a 3D T1-weighted fast spoiled gradient echo sequence [repetition time (TR) 7.8 ms, echo time (TE) 3 ms, inversion time (TI) 450 ms, 12° flip angle (FA), sagittal 1.0-mm-thick slices, 0.94 × 0.94 mm in-plane resolution].

MEG data were recorded using a 306-channel whole-head system (Elekta Neuromag Oy) while participants were in a supine position in a magnetically shielded room (Vacuumschmelze). Data were recorded during no-task eyes-open (3 min) and eyes-closed (5 min) conditions, using a sample frequency of 1,250 Hz and online anti-aliasing (410 Hz) and high-pass (0.1 Hz) filters. The head position relative to the MEG sensors was recorded continuously using the signals from four head localization coils. The head localization coil positions were digitized, as was the outline of the participants scalp (~500 points), using a 3D digitizer (Fastrak; Polhemus).

Channels that were malfunctioning, for example due to excessive noise, were identified by visual inspection of the data (mean number of excluded channels was six, range 2–11), and removed before applying the tSSS in MaxFilter software (version 2.2.15; Elekta Neuromag Oy) (56). The tSSS filter was used to remove artifacts that SSS without temporal extension would fail to discard, typically from noise sources near the head, using a subspace correlation limit of 0.9 and a sliding window of 10 s.

The scalp surfaces of all subjects were coregistered to their structural MRIs using a surface-matching procedure, with an estimated resulting accuracy of 4 mm (62). A single sphere was fitted to the outline of the scalp as obtained from the coregistered MRI, which was used as a volume conductor model for the beamformer approach described in *Beamforming*.

Beamforming. An atlas-based beamformer approach was adopted to project MEG data from sensor level to source space (14). First, the coregistered MRI was spatially normalized to a template MRI using the New Segment toolbox in SPM8 (63). The AAL atlas was used to label the voxels in a subject's normalized coregistered MRI (64). Subcortical structures were removed, as MEG is most sensitive to cortical regions (65), and the voxels in the remaining 78 cortical regions of interest (ROIs) were used for further analysis (66), after inverse transformation to the patient's coregistered MRI. Next, neuronal activity in the labeled voxels was reconstructed using a scalar beamformer implementation (beamformer, version 2.1.28; Elekta Neuromag Oy) similar to Synthetic Aperture Magnetometry (67).

This beamformer sequentially reconstructs the activity for each voxel in a predefined grid covering the entire brain (spacing 2 mm) by selectively weighting the contribution from each MEG sensor to a voxel's time series. The beamformer weights are based on the data covariance matrix and the forward solution (lead field) of a dipolar source at the voxel location (30, 67, 68). A time window of, on average, 287 s (range 139–394 s) was used to compute the data covariance matrix. Singular value truncation was used when inverting the data covariance matrix to deal with the rank deficiency of the data after SSS (~70 components).

Each ROI in the atlas contains many voxels, and the number of voxels per ROI differs. To obtain a single time series for an ROI, we used each ROI's centroid as representative for that ROI, with the centroid defined here as the voxel within the ROI that is nearest, in terms of Euclidean distance, to all other voxels in the ROI [see Fig. S6 and Table S6 for comparison with an approach based on selection of the voxel with maximum activation (14)].

The broadband (0.5–48 Hz) time series were projected through the normalized (69) broadband beamformer weights for each target voxel (i.e., centroid) to obtain a time series for an ROI. From these time series, the first 20 artifact-free epochs, containing 4,096 samples (3.2768 s), were selected to obtain stable results (70). These time series were then filtered in classical EEG/MEG frequency bands [delta (0.5–4 Hz), theta (4–8 Hz), alpha1 (8–10 Hz), alpha2 (10–13 Hz), beta (13–30 Hz), and lower gamma (30–48 Hz)], using an offline discrete fast Fourier transform filter that does not distort the phases (BrainWave, version 0.9.150.6; home.kpn.nl/stam7883/brainwave.html). Subsequently, the instantaneous phase for each time series was computed by taking the argument of the analytic signal as computed using the Hilbert transform (see e.g., ref. 71 for details).

PTE. The information flow between ROIs was estimated using the PTE, which has recently been introduced by Lobier et al. (35). PTE is based on the same principle as Wiener–Granger Causality, namely that a source signal has a causal influence on a target signal if knowing the past of both signals improves the ability to predict the target's future compared with knowing only the target's past (72, 73). In the framework of Information Theory, this can best be understood in terms of uncertainty: A source signal has a causal influence on a target signal if the uncertainty of the target signal conditioned on both its own past and that of the source signals is smaller than the uncertainty of the target signal conditioned only on its own past. If the uncertainty of a target signal Y at a delay δ is expressed in terms of Shannon Entropy (74), then the Transfer Entropy (TE) from source signal X to target signal Y can be expressed as (75)

$$\mathrm{TE}_{xy} = \sum p(Y_{t+\delta}, Y_t, X_t) \log\left(\frac{p(Y_{t+\delta}|Y_t, X_t)}{p(Y_{t+\delta}|Y_t)}\right) \quad [1]$$

where the definition for Shannon Entropy (74), $H(Y_{t+\delta}) = -\sum p(Y_{t+\delta}) \log p(Y_{t+\delta})$, was used, and the sum runs over all discrete time steps t.

For observed data, estimation of the probabilities in Eq. **1** is time-consuming and requires fine-tuning of several parameters (76). To solve these problems, Staniek and Lehnertz proposed to estimate transfer entropy by converting observed time series into sequences of symbols (77). In the same spirit, time series can be described in terms of their amplitudes and instantaneous phases (78), following which transfer entropy can be estimated from the time series of the instantaneous phases (PTE), at low computational cost (35). Dropping the subscript t for clarity, and using the fact that $p(Y_\delta, Y) = p(Y_\delta)\, p(Y)$, the PTE becomes

$$\mathrm{PTE}_{xy} = \sum p(Y_\delta) p(Y) p(X) \log\left(\frac{p(Y_\delta|Y, X)}{p(Y_\delta|Y)}\right) \quad [2]$$

where the probabilities are obtained by building histograms of occurrences of single, pairs or triplets of phase estimates in an epoch (35). The number of bins in the histograms was set as $e^{0.626+0.4\ln(N_s-\delta-1)}$ (78), and the prediction delay δ was set as $(N_s \times N_{ch})/N_{\pm}$, with N_s and N_{ch} the number of samples and channels (ROIs), respectively, and $N_{\pm}$ the number of times the phase changes sign across time and channels.

Finally, because the PTE does not have a meaningful upper bound (35), and to reduce biases, i.e., the effect of having (small) nonzero PTE values in situations when there is no actual information flow, we normalized the PTE,

$$\mathrm{dPTE}_{xy} = \frac{\mathrm{PTE}_{xy}}{\mathrm{PTE}_{xy} + \mathrm{PTE}_{yx}}. \quad [3]$$

The value of dPTE_{xy} ranges between 0 and 1. When information flows preferentially from time series X to time series Y, $0.5 < \mathrm{dPTE}_{xy} \leq 1$. When information flows preferentially toward X from Y, $0 \leq \mathrm{dPTE}_{xy} < 0.5$. In the case of no preferential direction of information flow, $\mathrm{dPTE}_{xy} = 0.5$.

It should be noted that our implementation differs slightly from Lobier et al. (35) in the way the number of bins, the prediction delay, and the normalization were computed. However, Lobier et al. showed that dPTE is robust against the a priori choice of the prediction delay, or the method used to construct the (conditional) probability distributions, and these differences in implementation should therefore not have affected our results.

Statistical Analysis. For each frequency band and subject separately, the dPTE matrices were averaged over the 20 epochs, yielding one matrix per subject. These were then averaged over subjects. The average dPTE value was subsequently computed for each ROI; that is, the average preferred direction of information flow for a region was also computed.

To establish if there was a consistent pattern of information flow, a PAx was computed as follows:

$$\mathrm{PAx} = \left\{\overline{\mathrm{dPTE}}_{xy}\right\}_{\mathrm{posterior}} - \left\{\overline{\mathrm{dPTE}}_{xy}\right\}_{\mathrm{anterior}} \quad [4]$$

where the dPTE was averaged over a set of posterior and anterior regions, respectively (see Table S1). A positive PAx indicates preferential flow from posterior regions toward anterior regions, and negative PAx preferential flow from anterior regions toward posterior regions. PAx was normalized by the absolute maximum PAx value that could have been obtained with the dPTE values for these individual ROIs. Significance of the PAx was assessed using randomization testing, where the average dPTE values were permuted across the ROIs, after which the PAx was computed. This was repeated 5,000 times to build a distribution of surrogate PAx values against which the observed PAx was tested ($P < 0.05$).

ACKNOWLEDGMENTS. We thank Nico Akemann, Ndedi Sijsma, Karin Plugge, Marlous van den Hoek, and Peter-Jan Ris for the MEG acquisitions, as well as the three anonymous reviewers for their constructive comments during the preparation of this manuscript. This work was supported by a private sponsorship to the VUmc MS Center Amsterdam. The MS Center is sponsored through a program grant by the Dutch MS Research Foundation (Grant 09-358d).

1. Tononi G, Edelman GM, Sporns O (1998) Complexity and coherency: Integrating information in the brain. *Trends Cogn Sci* 2(12):474–484.
2. Bullmore E, Sporns O (2012) The economy of brain network organization. *Nat Rev Neurosci* 13(5):336–349.
3. Stam CJ (2014) Modern network science of neurological disorders. *Nat Rev Neurosci* 15(10):683–695.
4. Mountcastle VB (1997) The columnar organization of the neocortex. *Brain* 120(Pt 4): 701–722.
5. Kanwisher N (2010) Functional specificity in the human brain: A window into the functional architecture of the mind. *Proc Natl Acad Sci USA* 107(25):11163–11170.
6. Fries P (2005) A mechanism for cognitive dynamics: Neuronal communication through neuronal coherence. *Trends Cogn Sci* 9(10):474–480.
7. Varela F, Lachaux J-P, Rodriguez E, Martinerie J (2001) The brainweb: Phase synchronization and large-scale integration. *Nat Rev Neurosci* 2(4):229–239.
8. Singer W (1999) Neuronal synchrony: A versatile code for the definition of relations? *Neuron* 24(1):49–65.
9. Canolty RT, et al. (2010) Oscillatory phase coupling coordinates anatomically dispersed functional cell assemblies. *Proc Natl Acad Sci USA* 107(40):17356–17361.
10. Friston KJ (2011) Functional and effective connectivity: a review. *Brain Connect* 1(1): 13–36.
11. Brookes MJ, et al. (2011) Investigating the electrophysiological basis of resting state networks using magnetoencephalography. *Proc Natl Acad Sci USA* 108(40): 16783–16788.
12. Mantini D, Perrucci MG, Del Gratta C, Romani GL, Corbetta M (2007) Electrophysiological signatures of resting state networks in the human brain. *Proc Natl Acad Sci USA* 104(32):13170–13175.
13. Damoiseaux JS, et al. (2006) Consistent resting-state networks across healthy subjects. *Proc Natl Acad Sci USA* 103(37):13848–13853.
14. Hillebrand A, Barnes GR, Bosboom JL, Berendse HW, Stam CJ (2012) Frequency-dependent functional connectivity within resting-state networks: An atlas-based MEG beamformer solution. *Neuroimage* 59(4):3909–3921.
15. Webb JT, Ferguson MA, Nielsen JA, Anderson JS (2013) BOLD Granger causality reflects vascular anatomy. *PLoS One* 8(12):e84279.
16. Ramsey JD, et al. (2010) Six problems for causal inference from fMRI. *Neuroimage* 49(2):1545–1558.
17. Ito J, Nikolaev AR, van Leeuwen C (2005) Spatial and temporal structure of phase synchronization of spontaneous alpha EEG activity. *Biol Cybern* 92(1):54–60.
18. Nolte G, et al. (2008) Robustly estimating the flow direction of information in complex physical systems. *Phys Rev Lett* 100(23):234101.
19. Lee H, Mashour GA, Noh GJ, Kim S, Lee U (2013) Reconfiguration of network hub structure after propofol-induced unconsciousness. *Anesthesiology* 119(6): 1347–1359.
20. van Dellen E, et al. (2014) Decreased functional connectivity and disturbed directionality of information flow in the electroencephalography of intensive care unit patients with delirium after cardiac surgery. *Anesthesiology* 121(2):328–335.
21. van Straaten EC, et al. (2015) Disturbed phase relations in white matter hyperintensity based vascular dementia: an EEG directed connectivity study. *Clin Neurophysiol* 126(3):497–504.
22. Moon JY, Lee U, Blain-Moraes S, Mashour GA (2015) General relationship of global topology, local dynamics, and directionality in large-scale brain networks. *PLOS Comput Biol* 11(4):e1004225.

23. Stam CJ, van Straaten EC (2012) Go with the flow: Use of a directed phase lag index (dPLI) to characterize patterns of phase relations in a large-scale model of brain dynamics. *Neuroimage* 62(3):1415–1428.
24. Osterhage H, Mormann F, Wagner T, Lehnertz K (2008) Detecting directional coupling in the human epileptic brain: Limitations and potential pitfalls. *Phys Rev E Stat Nonlin Soft Matter Phys* 77(1 Pt 1):011914.
25. Guevara R, et al. (2005) Phase synchronization measurements using electroencephalographic recordings: What can we really say about neuronal synchrony? *Neuroinformatics* 3(4):301–314.
26. Pascual-Marqui RD, et al. (2014) Assessing direct paths of intracortical causal information flow of oscillatory activity with the isolated effective coherence (iCoh). *Front Hum Neurosci* 8:448.
27. Babiloni C, et al. (2008) White matter vascular lesions are related to parietal-to-frontal coupling of EEG rhythms in mild cognitive impairment. *Hum Brain Mapp* 29(12):1355–1367.
28. Blinowska KJ, Kuś R, Kamiński M (2004) Granger causality and information flow in multivariate processes. *Phys Rev E Stat Nonlin Soft Matter Phys* 70(5 Pt 1):050902.
29. Baillet S, Mosher JC, Leahy RM (2001) Electromagnetic brain mapping. *IEEE Signal Process Mag* 18(6):14–30.
30. Hillebrand A, Singh KD, Holliday IE, Furlong PL, Barnes GR (2005) A new approach to neuroimaging with magnetoencephalography. *Hum Brain Mapp* 25(2):199–211.
31. Pereda E, Quiroga RQ, Bhattacharya J (2005) Nonlinear multivariate analysis of neurophysiological signals. *Prog Neurobiol* 77(1-2):1–37.
32. Blinowska KJ (2011) Review of the methods of determination of directed connectivity from multichannel data. *Med Biol Eng Comput* 49(5):521–529.
33. Greenblatt RE, Pflieger ME, Ossadtchi AE (2012) Connectivity measures applied to human brain electrophysiological data. *J Neurosci Methods* 207(1):1–16.
34. Sakkalis V (2011) Review of advanced techniques for the estimation of brain connectivity measured with EEG/MEG. *Comput Biol Med* 41(12):1110–1117.
35. Lobier M, Siebenhühner F, Palva S, Palva JM (2014) Phase transfer entropy: A novel phase-based measure for directed connectivity in networks coupled by oscillatory interactions. *Neuroimage* 85(Pt 2):853–872.
36. Buckner RL, Andrews-Hanna JR, Schacter DL (2008) The brain's default network: Anatomy, function, and relevance to disease. *Ann N Y Acad Sci* 1124:1–38.
37. Raichle ME, Snyder AZ (2007) A default mode of brain function: A brief history of an evolving idea. *Neuroimage* 37(4):1083–1090.
38. Buzsáki G (2010) Neural syntax: Cell assemblies, synapsembles, and readers. *Neuron* 68(3):362–385.
39. Hebb DO (1949) *The Organization of Behavior* (Wiley, New York).
40. Tóth B, et al. (2014) Frontal midline theta connectivity is related to efficiency of WM maintenance and is affected by aging. *Neurobiol Learn Mem* 114:58–69.
41. von Stein A, Sarnthein J (2000) Different frequencies for different scales of cortical integration: From local gamma to long range alpha/theta synchronization. *Int J Psychophysiol* 38(3):301–313.
42. Edelman GM, Gally JA (2013) Reentry: A key mechanism for integration of brain function. *Front Integr Neurosci* 7:63.
43. Clayton MS, Yeung N, Cohen Kadosh R (2015) The roles of cortical oscillations in sustained attention. *Trends Cogn Sci* 19(4):188–195.
44. Palva S, Palva JM (2007) New vistas for alpha-frequency band oscillations. *Trends Neurosci* 30(4):150–158.
45. Bastos AM, et al. (2015) Visual areas exert feedforward and feedback influences through distinct frequency channels. *Neuron* 85(2):390–401.
46. Frey JN, Ruhnau P, Weisz N (2015) Not so different after all: The same oscillatory processes support different types of attention. *Brain Res* 1626:183–197.
47. Zheng C, Colgin LL (2015) Beta and gamma rhythms go with the flow. *Neuron* 85(2): 236–237.
48. Sirota A, et al. (2008) Entrainment of neocortical neurons and gamma oscillations by the hippocampal theta rhythm. *Neuron* 60(4):683–697.
49. Benchenane K, Tiesinga PH, Battaglia FP (2011) Oscillations in the prefrontal cortex: A gateway to memory and attention. *Curr Opin Neurobiol* 21(3):475–485.
50. van Kerkoerle T, et al. (2014) Alpha and gamma oscillations characterize feedback and feedforward processing in monkey visual cortex. *Proc Natl Acad Sci USA* 111(40): 14332–14341.
51. Tomasi D, Volkow ND (2011) Association between functional connectivity hubs and brain networks. *Cereb Cortex* 21(9):2003–2013.
52. Akam T, Kullmann DM (2010) Oscillations and filtering networks support flexible routing of information. *Neuron* 67(2):308–320.
53. de Haan W, Mott K, van Straaten EC, Scheltens P, Stam CJ (2012) Activity dependent degeneration explains hub vulnerability in Alzheimer's disease. *PLOS Comput Biol* 8(8):e1002582.
54. Schoffelen J-M, Gross J (2014) Studying dynamic neural interactions with MEG. *Magnetoencephalography: From Signals to Dynamic Cortical Networks*, eds Supek S, Aine CJ (Springer, New York), pp 405–427.
55. Litvak V, et al. (2010) Optimized beamforming for simultaneous MEG and intracranial local field potential recordings in deep brain stimulation patients. *Neuroimage* 50(4): 1578–1588.
56. Taulu S, Simola J (2006) Spatiotemporal signal space separation method for rejecting nearby interference in MEG measurements. *Phys Med Biol* 51(7):1759–1768.
57. Muthukumaraswamy SD, Singh KD (2011) A cautionary note on the interpretation of phase-locking estimates with concurrent changes in power. *Clin Neurophysiol* 122(11):2324–2325.
58. Akam T, Kullmann DM (2014) Oscillatory multiplexing of population codes for selective communication in the mammalian brain. *Nat Rev Neurosci* 15(2):111–122.
59. Tewarie P, et al. (2014) Disruption of structural and functional networks in long-standing multiple sclerosis. *Hum Brain Mapp* 35(12):5946–5961.
60. Tewarie P, et al. (2014) Structural degree predicts functional network connectivity: A multimodal resting-state fMRI and MEG study. *Neuroimage* 97:296–307.
61. Tewarie P, et al. (2015) Functional brain networks: Linking thalamic atrophy to clinical disability in multiple sclerosis, a multimodal fMRI and MEG study. *Hum Brain Mapp* 36(2):603–618.
62. Whalen C, Maclin EL, Fabiani M, Gratton G (2008) Validation of a method for coregistering scalp recording locations with 3D structural MR images. *Hum Brain Mapp* 29(11):1288–1301.
63. Weiskopf N, et al. (2011) Unified segmentation based correction of R1 brain maps for RF transmit field inhomogeneities (UNICORT). *Neuroimage* 54(3):2116–2124.
64. Tzourio-Mazoyer N, et al. (2002) Automated anatomical labeling of activations in SPM using a macroscopic anatomical parcellation of the MNI MRI single-subject brain. *Neuroimage* 15(1):273–289.
65. Hillebrand A, Barnes GR (2002) A quantitative assessment of the sensitivity of whole-head MEG to activity in the adult human cortex. *Neuroimage* 16(3 Pt 1):638–650.
66. Gong G, et al. (2009) Mapping anatomical connectivity patterns of human cerebral cortex using in vivo diffusion tensor imaging tractography. *Cereb Cortex* 19(3): 524–536.
67. Robinson SE, Vrba J (1999) Functional neuroimaging by Synthetic Aperture Magnetometry (SAM). *Recent Advances in Biomagnetism*, eds Yoshimoto T, Kotani M, Kuriki S, Karibe H, Nakasato N (Tohoku Univ Press, Sendai, Japan), pp 302–305.
68. Van Veen BD, van Drongelen W, Yuchtman M, Suzuki A (1997) Localization of brain electrical activity via linearly constrained minimum variance spatial filtering. *IEEE Trans Biomed Eng* 44(9):867–880.
69. Cheyne D, Bostan AC, Gaetz W, Pang EW (2007) Event-related beamforming: A robust method for presurgical functional mapping using MEG. *Clin Neurophysiol* 118(8): 1691–1704.
70. van Diessen E, et al. (2015) Opportunities and methodological challenges in EEG and MEG resting state functional brain network research. *Clin Neurophysiol* 126(8): 1468–1481.
71. Stam CJ, Nolte G, Daffertshofer A (2007) Phase lag index: Assessment of functional connectivity from multi channel EEG and MEG with diminished bias from common sources. *Hum Brain Mapp* 28(11):1178–1193.
72. Wiener N (1956) The theory of prediction. *Modern Mathematics for the Engineer: First Series*, ed Bechenbach E (McGraw-Hill, New York), pp 165–190.
73. Granger CWJ (1969) Investigating causal relations by econometric models and cross-spectral methods. *Econometrica* 37(3):424–438.
74. Shannon CE (1948) A mathematical theory of communication. *Bell Syst Tech J* 27(3): 379–423.
75. Schreiber T (2000) Measuring information transfer. *Phys Rev Lett* 85(2):461–464.
76. Wibral M, et al. (2011) Transfer entropy in magnetoencephalographic data: quantifying information flow in cortical and cerebellar networks. *Prog Biophys Mol Biol* 105(1-2):80–97.
77. Staniek M, Lehnertz K (2008) Symbolic transfer entropy. *Phys Rev Lett* 100(15):158101.
78. Rosenblum MG, Pikovsky AS, Kurths J, Schäfer C, Tass P (2001) Phase synchronization: From theory to data analysis. *Neuro-Informatics and Neural Modeling,* Handbook of Biological Physics, ed Hoff AJ (Elsevier, New York), Vol 4, pp 279–321.
79. Kaminski M, Blinowska KJ (2014) Directed Transfer Function is not influenced by volume conduction-inexpedient pre-processing should be avoided. *Front Comput Neurosci* 8:61.
80. Vinck M, et al. (2015) How to detect the Granger-causal flow direction in the presence of additive noise? *Neuroimage* 108:301–318.
81. Friston KJ, Harrison L, Penny W (2003) Dynamic causal modelling. *Neuroimage* 19(4): 1273–1302.
82. Daunizeau J, David O, Stephan KE (2011) Dynamic causal modelling: A critical review of the biophysical and statistical foundations. *Neuroimage* 58(2):312–322.
83. Friston KJ, Li B, Daunizeau J, Stephan KE (2011) Network discovery with DCM. *Neuroimage* 56(3):1202–1221.
84. Kamiński MJ, Blinowska KJ (1991) A new method of the description of the information flow in the brain structures. *Biol Cybern* 65(3):203–210.
85. Baccalá LA, Sameshima K (2001) Partial directed coherence: A new concept in neural structure determination. *Biol Cybern* 84(6):463–474.
86. Hadjipapas A, et al. (2009) Can we observe collective neuronal activity from macroscopic aggregate signals? *Neuroimage* 44(4):1290–1303.
87. Vrba J, Robinson SE (2001) Signal processing in magnetoencephalography. *Methods* 25(2):249–271.
88. Nichols TE, Holmes AP (2002) Nonparametric permutation tests for functional neuroimaging: A primer with examples. *Hum Brain Mapp* 15(1):1–25.
89. Zobay O, Palmer AR, Hall DA, Sereda M, Adjamian P (2015) Source space estimation of oscillatory power and brain connectivity in tinnitus. *PLoS One* 10(3):e0120123.
90. Barnes GR, Hillebrand A (2003) Statistical flattening of MEG beamformer images. *Hum Brain Mapp* 18(1):1–12.